Reaction Chemistry & Engineering

ROYAL SOCIETY OF CHEMISTRY

PAPER

View Article Online
View Journal | View Issue

Cite this: *React. Chem. Eng.*, 2026, 11, 449

Enabling easy access to flow chemistry: stainless steel reactors with a heating and cooling device printed using a standard FDM 3D printer

Christian C. Mahlenbrey, † Florian Menzel, † Thomas Ziegler and Jochen M. Neumaier *

Continuous production of chemicals under flow conditions is one of the most modern synthesis methods in the industry. The industry takes full advantage by using primarily stainless steel reactors. These industrial reactors are very expensive, and the more cost-effective alternatives, such as coiled tubes, often lack sufficient mixing capacities and are not suitable for laboratory work due to their large volume. Herein we present 3D-printed stainless steel (316L) flow reactors, which could be printed using a standard desktop FDM printer, making this technology easily accessible for every research facility. Thermal conductivity is one of the major advantages in choosing stainless steel as the reactor material. Therefore, we developed an application that allows the reactor to be heated or cooled directly, making the device very compact and easy to handle. The reactor can be heated directly up to 200 °C with a heating element, and the cooling can be accomplished using a Peltier element reaching temperatures under −20 °C. To investigate the functionality of the microreactors, we performed a Diels–Alder reaction with methyl vinyl ketone and a cannabinoid derivative at high temperatures and a subsequent reduction of the carbonyl group with DIBAL-H at low temperatures. In addition to its high thermal conductivity, stainless steel also features favorable chemical and mechanical resistance, highlighting the need for a convenient and simple way to manufacture such reactors. With this technology, we aim to provide a solution that enhances usability and amplifies the impact of flow chemistry in research.

Received 25th July 2025,
Accepted 28th October 2025

DOI: 10.1039/d5re00326a

rsc.li/reaction-engineering

Introduction

In the last three decades, microfluidics has attracted more attention in chemistry, biochemistry, and instrumental analysis, pushing flow chemistry research to the next level.[1–4] Moreover, this rapidly growing interest can be justified by several advantages of this method. Unlike conventional batch reactors, continuous-flow microreactors typically exhibit improved heat and mass transfer as well as better controllability due to higher surface-to-volume ratios and shorter mixing times.[5,6] Additionally, multiple reaction steps, purification steps, and analyses can be sequenced in a single continuous production process.[7] Moreover, avoiding direct contact with toxic or hazardous reagents and minimizing their amount improves the overall chemical safety in the laboratory.[8] Of all the microfluidic components, microreactors are one of the most important components that can drastically change the overall performance of the entire system. They are commercially available in various inert materials such as glass, stainless steel, or ceramics.[9] Typically, these reactors are manufactured using mass-production techniques such as micromachining, etching, and laser ablation and offer little opportunity for customization. The ability to customize reactors to reaction conditions, rather than having to adapt processes to commercially available reactors, has interested researchers for some time. Consequently, three-dimensional (3D) printing techniques are attracting much attention as a simple additive manufacturing technology for 3D objects.[10–15] It enables the development of microfluidic reactors as well as quick adaptation *via* design modification using CAD software on desktop computers. Another advantage of 3D-printed reactors over simple coiled tube reactors is the rapid and cost-effective production of complex internal geometries that are difficult or impossible to achieve with coiled tubes.[10] These geometric freedoms can improve the mixing efficiency, reduce dead volume in multi-step sequences, and enable integrated sensor connections and thermal interfaces.[16,17] Although 3D printing has many advantages, applications for building microreactors are still astonishingly uncommon.[18] Most 3D-printed microreactors are fabricated using fused deposition modeling (FDM)[19,20] and stereolithography (SLA).[21] Though being comparatively

Institute of Organic Chemistry, University of Tübingen, Auf der Morgenstelle 18, 72076 Tübingen, Germany. E-mail: jochen.neumaier@uni-tuebingen.de
† Shared first authorship.

inexpensive, those methods are currently limited to polymer-based materials, which have low stability to a range of reagents and common organic solvents. In addition, the low-temperature resistance of these materials further narrows the range of potential applications. In recent years, metal 3D printing processes such as selective laser melting (SLM),[22] electron beam melting (EBM),[23,24] and binder jetting[25,26] have been developed significantly. Both EBM and binder jetting have already been applied to fabricate metal microreactors, such as a microrectification apparatus,[27] and microreactor components, for instance, structured reactor inserts for heterogeneous catalysis.[28–30] However, 3D-printed microreactors designed for operation under medium- to high-pressure conditions are more frequently manufactured by SLM technology. Several 3D-printed 316L stainless steel reactors have already been successfully produced using this technology.[31–35] Those reactors provide thermal conductivity as well as chemical, mechanical, and thermal stability, which are often required for organic synthesis. However, this fabrication method requires an extremely expensive SLM printer (over 100k €). The possibility of manufacturing stainless steel reactors using an inexpensive desktop FDM printer would significantly improve the development and increase their usage considerably. This can be achieved by using sinterable metal filaments (*e.g.* Ultrafuse 316L from BASF).[36,37]

Herein, we present a solution that allows us to design stainless steel reactors individually using a CAD program and manufacture them using a commercially available, inexpensive FDM desktop printer. We have also taken advantage of the reactor material and developed a technology that allows us to heat the reactor directly up to 200 °C and cool it to approximately −20 °C due to its excellent thermal conductivity (Fig. 1).[38]

For the heating process, we used a commercially available positive-temperature-coefficient (PTC) heating thermistor and an Arduino-driven control unit. The PTC-heating element refers to an electrical component with temperature-dependent characteristics. The self-regulating property of the PTC-heating element makes the heating particularly safe and reliable.[39,40]

Cooling, in contrast, can be accomplished using a Peltier element (thermoelectric cooler) with the same temperature controller used for heating. The Peltier effect was named after its discoverer, the French physicist J. C. A. Peltier, who observed heat emission and absorption at the contact between two different conducting media when a direct electric current flows through this contact.[41] If electricity is passed through two series-connected contacts of semiconductors, thermal energy must be absorbed at one contact point, and at the other point, this energy is released in the form of heat.[42]

Both temperature elements are commercially available and, in conjunction with a temperature sensor, the temperatures can be precisely set and controlled with the presented control unit.

Results and discussion

All components of the microreactors, including the guide rails for tube connections, were fabricated using a standard desktop FDM 3D printer, specifically the Qidi X-CF Pro. It was crucial to us that no high-end 3D printers such as SLM systems were required, ensuring that the reactors can be manufactured with virtually any FDM 3D printer. As filament we used a 1.75 mm Ultrafuse 316L from BASF.[43,44] After manually finishing, the printed parts were sintered by Elnik Systems GmbH. The sintering process was carried out entirely by the external company specializing in this field. The parameters of the debinding and sintering process can be found in the SI. Fig. 2 provides an overview of the entire process, from initial printing to the sintered reactor. It should be noted that the components shrink during the sintering process. Therefore, the reactors must be scaled to 120% on the *X* and *Y* axes and to 124% on the *Z* axis before printing. To ensure a consistent metal block without gaps, printing must be done very slowly (15 mm s^{-1}) and with an increased filament flow ratio (extrusion multiplier). Flow ratios of 1.00, 1.05 and 1.10 were tested. If the flow ratios were too low, minimal gaps could sometimes be observed between the extrusion lines, which led to a leaking reactor after sintering. For this reason, the flow ratio should be at least 1.10. A more detailed manufacturing instruction can be found in the SI.

With these parameters, it was possible to print microreactors with mixing channels with the same parallel

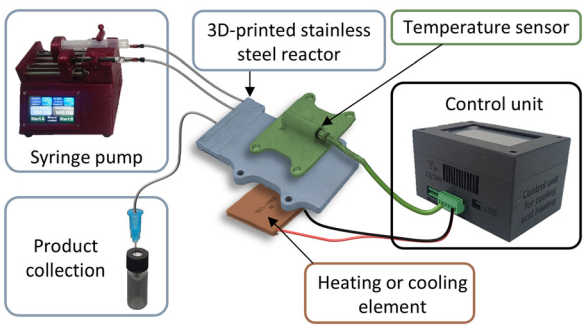

Fig. 1 Schematic of the microfluidic system.

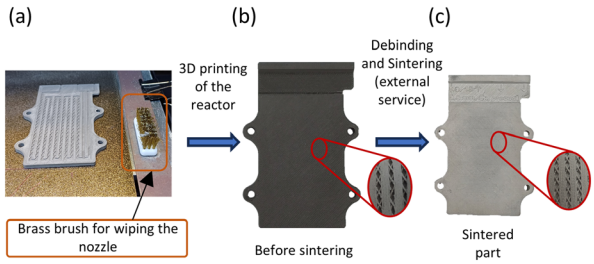

Fig. 2 Process of the production of the stainless steel reactor: 3D printing with BASF Ultrafuse 316L (a); before sintering (b); and the sintered reactor (c).

cross geometry as published previously. With this geometry, we were previously able to demonstrate that, unlike small coiled tubes, we can ensure good mixing behavior.[14] The geometry used is shown in Fig. 3, and was printed remarkably well by the printer. The mixing channels remained unchanged after the sintering process.

Warping is a major problem while printing with a stainless steel filament, causing a round surface of the printed parts. This results in a bend during the sintering process, causing cracks and gabs in the microreactors. To ensure a flat base surface during the sintering process, the printed parts had to be sanded manually to a flat ground surface after the printing process (see SI). Moreover, all additional parts, like the brim around the printed parts and the support structure, had to be removed. Due to the necessity of printing with over-extrusion, a small excess of material is often present. To remove this material from the reactor, a script was added to the G-code that cleans the nozzle with a brass brush after each printed layer (Fig. 2a).

It was possible to produce different microreactors with volumes between 400 µL and 600 µL. We attempted to double the volume by stacking two mixing channels within a single reactor, but all efforts were unsuccessful due to various issues, including surface leakage and complete clogging of the reactor. The mixing zones could be reproduced well by the 3D printing process and were also still completely present after sintering (Fig. 2c). Due to the easy customizability, it was possible to receive reactors with different properties such as precooling zones or various internal volume to customize flow rates and therefore reaction times.

To ensure a flat surface at the tube connection part of the reactor, we had to polish the parts to a shiny flat surface after sintering.

To print the dovetail, one point in the reactor had to be a little thinner (Fig. 4a), which sometimes led to leaks. For this reason, a different mounting system was developed that eliminates the dovetail and uses a flat reactor that has the same thickness everywhere. Both systems are shown in Fig. 4. With this modified system, 3D printing is much

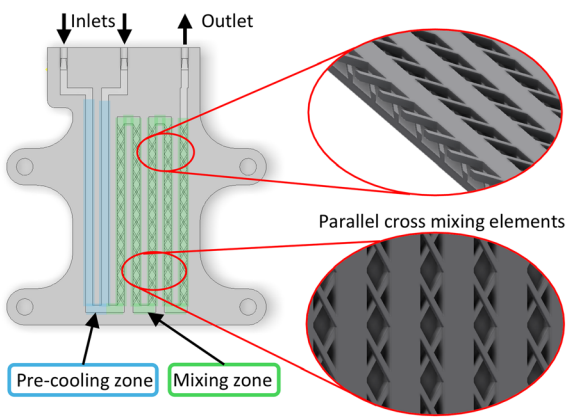

Fig. 3 Microreactor with a pre-cool zone and mixing zone with parallel cross mixing channels.

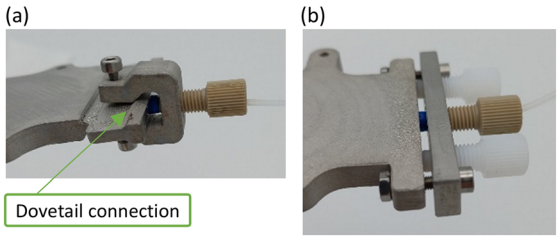

Fig. 4 Two connection options: Reactor with a dovetail and guide rail (a) and flat reactor with a connection bar (b).

easier, as the flat reactor no longer requires a support structure, and the results after sintering also show consistently good quality. The connection bar, which is loosely screwed to the reactor, can be made very easily from stainless steel by drilling and cutting the appropriate threads (see SI).

Development of the heating and cooling device

Another reason for using such a flat chip reactor is that it is very easy to install large-area temperature control. Therefore, we developed an integrated heating and cooling system to keep the footprint of the entire system small. The thermal control unit employs a 24 V PTC element for heating (up to 200 °C) and a 24 V Peltier module for cooling (down to approximately −20 °C). A PT1000 sensor (3-wire) with a MAX31865 amplifier from Adafruit is used for temperature measurement. The components are controlled with an Arduino Nano Every and a Nextion touch display. The graphical user interface has been designed to be very simple and intuitive to use (Fig. 5d). To ensure a stable 5 V power supply for the Arduino and the display, a LME78 5 V DC/DC converter is used with a 24 V input voltage. The system itself offers high flexibility, as it can also be operated with a 12 V supply when using 12 V PTC or Peltier elements.

To make the heating and cooling device as simple as possible and easy to build, we have made sure that only a small amount of soldering and wiring work is required. Therefore, we designed a central printed circuit board (PCB) in which all connections were routed and only the various components had to be soldered on. The PCB can be produced by commercial fabricators; the necessary Gerber files are provided in the SI. No additional soldering is required, as the cables are simply secured to the connectors with screws (Fig. 5c). Since the cables carry high currents (up to 6 A) and may overheat if they are too thin, it is important to use cables with a cross-sectional area of at least 1 mm^2, preferably 1.5 mm^2.

The temperature is controlled *via* a proportional-integral-derivative (PID) controller. Initially, the pulse width modulation (PWM) ports of the Arduino were used for this, but this led to a humming noise in the power supply unit. Therefore, the temperature control was achieved *via* an N-channel MOSFET transistor and a manually programmed PID controller. Instead of a frequency of 490 Hz, as used on

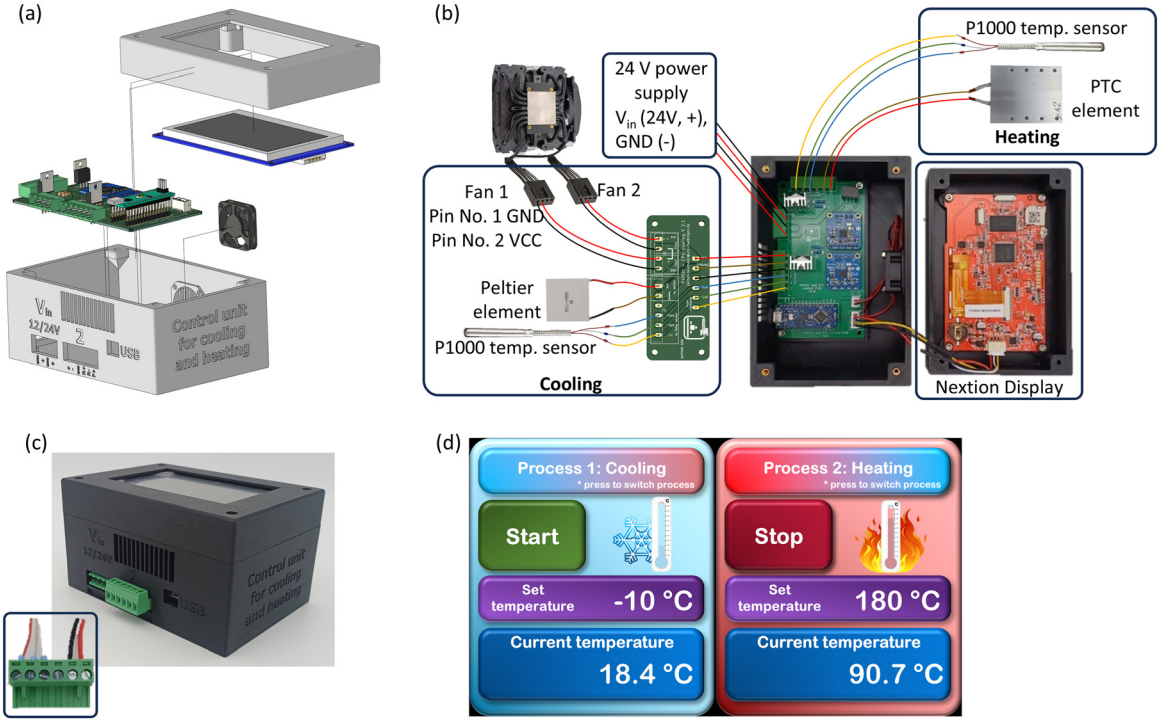

Fig. 5 Exploded view (a), schematic connection of the components (b), photograph of the control unit with a connector cable (c) and graphical user interface (GUI) (d).

the PWM ports of the Arduino Nano, a frequency of approximately 4 Hz was used (255 ms per duty cycle), which is completely sufficient for the slow reaction in temperature control. Detailed programming and calibration of the PID controller is described in the SI.

To achieve high reactor temperatures of up to 200 °C during chemical reactions, a 24 V PTC element with a power rating of 150 W was used (Fig. 6a). Despite the flexible input voltage, any other PTC element with a voltage range of 6–36 V and a flat surface can be used. However, the PID calibration has been performed for the 24 V PTC element and must be performed manually for another PTC element if necessary.

Cooling of the reactors was accomplished with a 24 V, 120 W Peltier element. As it has the same voltage of 24 V as the heating element, we were able to heat and cool two reactors at the same time. The Peltier element gets cold on one side and warm on the other. To dissipate the heat generated, we used two cooling systems: a water cooling system and an air cooling system.

The water cooling system (Fig. 6b) is very simple, space-saving and effective, but requires cooling water to work. With our laboratory cooling water, which had a temperature of 12 °C, we were able to achieve a minimum temperature of −22 °C. By isolating the reactor with an insulating foam, the temperature could be lowered by 3 K to −25 °C. With this setting, a reactor temperature of −20 °C could be maintained while flushing it with room-temperature solvents at a flow rate of 1 mL min^{-1}, without any thermal insulation.

If no cooling water is available, we developed an air cooling system (Fig. 6c). Therefore, a standard CPU cooler is attached to the hot side of the Peltier element and cooled with two 12 V fans. The two 12 V fans are connected in series, so that they can be operated with 24 V. For this purpose, a small PCB was developed, which distributes the current from the control unit to both the Peltier element and the fans (Fig. 5b). This air cooling system is of course not as effective as water cooling, but we were still able to cool the reactor down to −17 °C. The isolation of the reactor also resulted in a 3 K lower temperature of −20 °C.

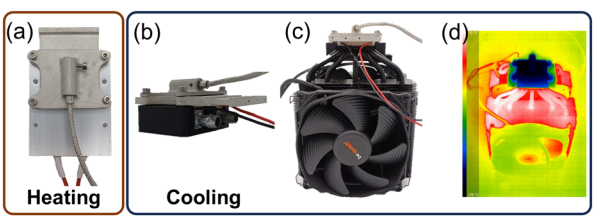

Fig. 6 Three-dimensional-printed reactor with a PTC element for heating (a), with Peltier element and water cooling (b), with Peltier element and air cooling (c) and thermal image during cooling process (d).

Diels–Alder reaction under flow conditions

Thanks to the straightforward handling of the stainless steel filament and the simplicity of the printing process, we were able to fabricate all components of the flow system using

stainless steel. This also allowed us to reproduce the previously published back pressure regulator (BPR) and pressure sensor (PS).[45]

With this setup, we were able to perform a Diels–Alder reaction[46] in continuous flow (Scheme 1). Therefore, we premixed a cannabinoid derivative **1** with methyl vinyl ketone (**2**) in toluene. The reactor was heated to the desired temperature and the flow rate was set according to the required reaction time. The premixed reaction solution was injected through a loop and a six-way valve into the continuous flow of toluene. Reaction temperatures were adjustable between 111 °C (the boiling point of toluene) and 200 °C. Temperatures above this range were not attainable due to excessive solvent vapor pressure, which disrupted the stability of the flow rate. Due to the nature of the performed Diels–Alder reaction, which yielded a mixture of the *cis* and *trans* isomer of **3** for the determination of the conversion of the reaction, we always used the sum of both products.

The reaction resulted in a much higher conversion rate in the flow system than in the conventional batch synthesis. We could achieve a six-time higher conversion rate in the flow system at 180 °C after 60 minutes than in the batch synthesis at reflux temperature. In addition to the improved conversion enabled by the higher temperatures achievable in the flow system, the Diels–Alder reaction at 111 °C reached the same conversion in the flow setup after 60 minutes as the batch synthesis did after three hours (Fig. 7).

The chosen reactor, with a total volume of 600 µL, allowed reaction times of up to 60 minutes. Extending the reaction time further was not possible, as the necessary reduction in flow rate risked disrupting continuous flow, which in turn severely diminished the conversion efficiency. This effect showed up when we tried to further extend the reaction time at the most promising temperature (180 °C). A reaction time of 120 minutes led to a dramatic drop in the conversion rate. This problem was caused by the syringe pump used in combination with the syringes. Larger syringes cause an inconsistent flow, which may have led to a pressure drop in the reactor. Using smaller syringes could solve this problem, but this was impractical due to the high reactor volume and was not investigated further.

A reaction time of 30 minutes at 180 °C and 200 °C resulted in a reduced conversion rate compared to lower and higher reaction times. Although we were able to reproduce this effect, we were not able to clarify the cause (Fig. 7).

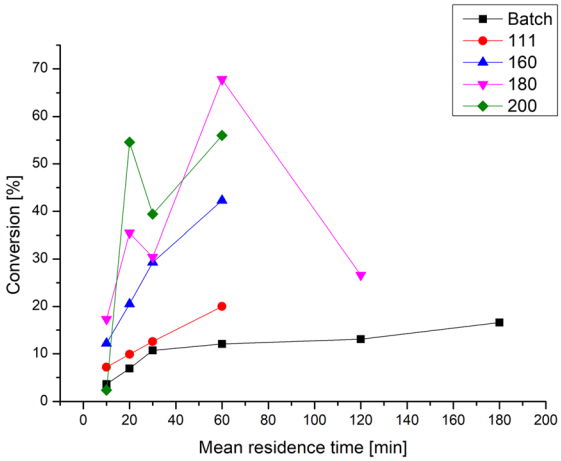

Fig. 7 Diels–Alder reaction for conversion to **3** at different temperatures and reaction times.

DIBAL-H reduction under flow conditions

To test the cooling device, we performed a reduction reaction of the carbonyl group from the previous Diels–Alder product **3** with DIBAL-H (Scheme 2). Therefore, we designed a reactor with a precool zone (Fig. 2) to ensure that the reactants are not mixed until they are cold.

The reactor was cooled to −10 °C and the flow rates were set according to residence times between 1 and 10 minutes in the mixing zone. The starting material **3** was injected through a 450 µL loop and a six-way valve into a continuous flow of toluene and DIBAL-H in toluene. The flow rate of the reducing agent was adjusted to 1.5 equivalents of DIBAL-H. After the reactor, the mixture was collected in a vessel filled with a concentrated solution of potassium sodium tartrate to quench the reaction. After a reaction time of 5 minutes, only traces of the educt were still present, which could no longer be isolated during workup. For workup, the collected reaction mixture was separated from the quenching solution and purified by column chromatography. After 2 minutes of reaction time,

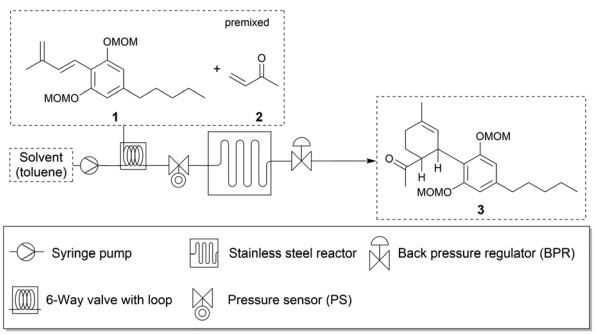

Scheme 1 Continuous flow reaction to the Diels–Alder product **3**.

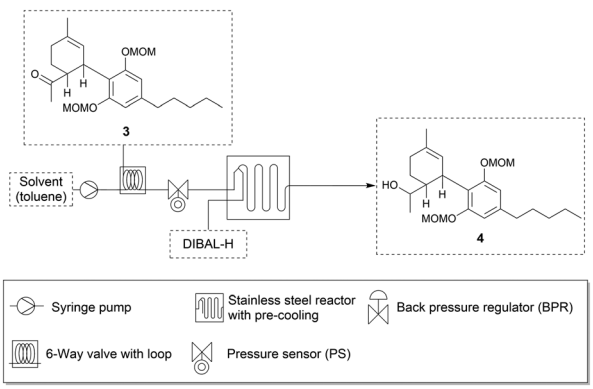

Scheme 2 Reduction to alcohol **4** under continuous flow conditions.

the conversion was 50%, after 5 minutes 94% and after 10 minutes no more starting material **3** could be detected by thin-layer chromatography or column chromatography.

Multistep reaction

After the two individual reactions were optimized, a multistep reaction consisting of the high-temperature Diels–Alder reaction and the subsequent low-temperature reduction was performed (Fig. 8). The temperature for the first reaction was set to 180 °C, and a 600 μL reactor was used. The cannabinoid derivative **1** was premixed with methyl vinyl ketone (**2**) and pumped through the preheated flow reactor using a syringe pump. The flow rate was set to a reaction time of 60 minutes and the pressure to 7 bar to prevent vaporization in the reactor. The resulting reaction mixture was further pumped through the second reactor, where a DIBAL-H solution in toluene was added through the second inlet. The flow rate of DIBAL-H was adjusted to 3.0 equivalents of DIBAL-H compared to the premixed starting material **1**. The reactor volume of the second reactor was 420 μL, resulting in a reaction time of 38 minutes for the second reaction. The conversion of the reaction was determined by gas chromatography and resulted in 82% of the reduced product **4**. It was found that 18% of the Diels–Alder product **3** was still left in the reaction mixture. No more starting material could be detected after the reaction. Due to the nature of the performed Diels–Alder reaction, the product was still a mixture of the *cis* and *trans* isomers of **4**.

Both reactions were carried out in our 3D-printed steel reactors and one control unit was used for both heating and cooling. Moreover, the BPR and the pressure sensor were 3D printed from stainless steel, so that no materials other than stainless steel and ETFE (tubing) come into contact with the chemicals.

Experimental

All 3D-printed parts were printed using a Qidi X-CF Pro FDM desktop printer. All printed stainless steel parts were printed using BASF Ultrafuse 316L, and the other parts were printed using PETG HF from Bambu Lab. The electronic parts of the cooling and heating controller are commercially available. Further instructions can be found in the SI.

Chemistry

NMR spectra were recorded using a Bruker "Avance 400" spectrometer and calibrated to the solvent signal ($CDCl_3$: ^1H 7.27 ppm, ^{13}C 77.0 ppm; CD_2Cl_2: ^1H 5.35 ppm, ^{13}C 54.0 ppm). A Bruker maXis 4G was used as the electron spray ionization mass spectrometer (HR-ESI-MS). GC measurements were made using a Hewlett Packard 5890 Series II gas chromatograph. Nitrogen was used as a carrier gas. All chromatographic separations were performed using a fused silica column (Agilent Technologies 122-5032) having specifications: length: 30 m; i.d.: 0.250 mm; film thickness; 0.25 μm; other GC conditions are: 5 μL of sample were injected into the GC column. The injector temperature was 280 °C. The column temperature program started at 40 °C for 3 minutes and changed to 300 °C at a rate of 10 °C min^{-1}. The temperature was maintained for 10 minutes. An FID sensor was used for detection.

All reagents and solvents were purchased from commercial suppliers and used without further purification, unless specified otherwise.

Batch synthesis of (4-acetyl-1-methylcyclohexen-3-yl)-1,3-di(methoxymethoxy)olivetol (3)

In a round-bottom flask, (*E*)-1,3-bis(methoxymethoxy)-(3-methylbuta-1,3-dien-1-yl)-olivetole (**1**) (50.0 mg; 0.15 mmol) was dissolved in wet toluene (5 mL). The solution was heated to reflux followed by the addition of methyl vinyl ketone (**2**) (0.015 mL; 0.18 mmol). The samples were taken from the solution at different times and analyzed by gas chromatography.

In a round-bottom flask, (*E*)-1,3-bis(methoxymethoxy)-(3-methylbuta-1,3-dien-1-yl)-olivetole (**1**) (100.0 mg; 0.15 mmol) was dissolved in wet toluene (15 mL). Methyl vinyl ketone (**2**)

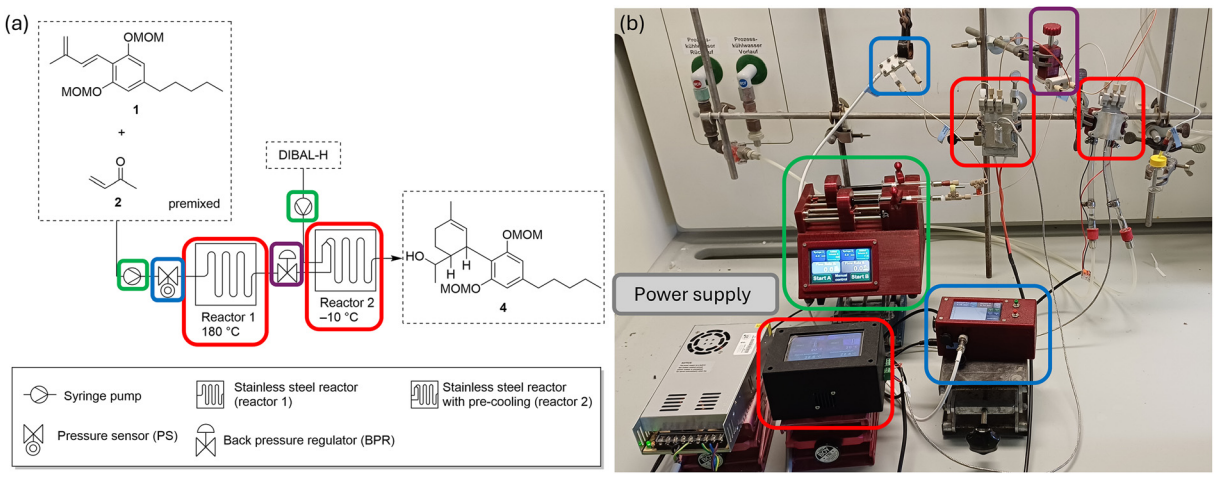

Fig. 8 Scheme (a) and picture (b) of the flow-multistep reaction to **4**.

(0.005 mL; 0.09 mmol) was added, and the solution was stirred under reflux for 8 h. The reaction mixture was then allowed to cool to room temperature and was stirred for a further 24 h. All volatile compounds were removed under reduced pressure and the resident was purified by flash chromatography (eluent: hexane/ethyl acetate 10/1; r_f = 0.20).

For analysis of the conversion, samples were taken from the solution at different times and analyzed by gas chromatography.

Trans: **^{1}H-NMR** (400 MHz, $CDCl_3$): δ [ppm] = 6.57 (s, 4H, H-4, 6), 5.33 (d, J = 1.6 Hz, 1H, H-1′), 5.03–5.14 (m, 4H, H-1-CH_2OCH$_3$, 3-CH_2OCH$_3$), 4.49–4.56 (m, 1H, H-5′), 3.47 (s, 6H, H-1-CH$_2$OCH_3, 3-CH$_2$OCH_3), 2.96 (s, 1H, H-6′), 2.47–2.53 (m, 2H, H-1″), 2.27–2.39 (m, 1H, H-4′), 2.12–2.21 (m, 1H, H-3′), 1.97–2.08 (m, 1H, H-3′), 1.86 (s, 3H, H-5′-COCH_3), 1.71 (s, 4H, H-2′-CH_3, 4′), 1.54–1.61 (m, 2H, H-2″), 1.26–1.38 (m, 4H, H-3″, 4″), 0.87–0.92 (m, 3H, H-5″) ppm.

^{13}C-NMR (100 MHz, $CDCl_3$): δ [ppm] = 211.2 (C-5′-*C*OCH$_3$), 156.4 (C-1, 3), 143.6 (C-5), 132.2 (C-2′), 122.8 (C-1′), 116.8 (C-2), 108.4 (C-4, 6), 94.7 (C-1-*C*H$_2$OCH$_3$, 3-*C*H$_2$OCH$_3$), 56.1 (C-1-CH$_2$O*C*H$_3$, 3-CH$_2$O*C*H$_3$), 51.5 (C-6′), 36.2 (C-1″), 32.3 (C-5′), 31.7 (C-3″), 30.9 (C-2″), 29.2 (C-5-COCH$_3$), 28.9 (C-3′), 23.8 (C-3′-*C*H$_3$), 22.5 (C-4″), 22.0 (C-4′), 14.0 (C-5″) ppm.

MS: m/z [M + Na]$^+$ = 427.24567.

Retention time: 27.3 min.

Cis: **^{1}H-NMR** (400 MHz, $CDCl_3$): δ [ppm] = 6.57 (s, 2H, H-4, 6), 5.21 (s, 1H, H-1′), 5.11 (dd, J = 16.1 Hz, J = 6.6 Hz, 4H, H-1-O*C*H$_2$OCH$_3$, 3-O*C*H$_2$OCH$_3$), 4.18–4.25 (m, 1H, H-4′), 3.47 (s, 6H, H-1-OCH_2OCH$_3$, 3-OCH_2OCH$_3$), 3.30–3.39 (m, 1H, H-6′), 2.51 (t, J = 7.8 Hz, 2H, H-1″), 1.99–2.20 (m, 2H, H-3′), 1.89–1.96 (m, 4H, H-5′, 4′-COCH_3), 1.78–1.88 (m, 1H, H-5′), 1.67 (s, 2H, H-2′-CH_3), 1.57 (s, 8H, H-2″), 1.25–1.37 (m, 7H, H-3″, 4″), 0.90 (t, J = 7.0 Hz, 4H, H-5″) ppm.

^{13}C-NMR (100 MHz, $CDCl_3$): δ [ppm] = 213.2 (C-4′-*C*OCH$_3$), 156.0 (C-1, 3), 143.2 (C-5), 131.2 (C-2′), 124.9 (C-1′), 118.6 (C-2), 108.6 (C-4, 6), 94.7 (C-1-O*C*H$_2$OCH$_3$, 3-O*C*H$_2$OCH$_3$), 56.1 (C-1-OCH$_2$O*C*H$_3$, 3-OCH$_2$O*C*H$_3$), 50.8 (C-6′), 36.2 (C-1″), 35.0 (C-4′), 31.7 (C-3″), 31.0 (C-2″), 29.6 (C-3′), 29.3 (C-4′-CO*C*H$_3$), 26.4 (C-5′), 23.3 (C-2′-*C*H$_3$), 22.5 (C-4″), 14.1 (C-5″) ppm.

MS: m/z [M + Na]$^+$ = 427.24567.

Retention time: 27.0 min.

Batch synthesis of (4-(1-hydroxyethyl)-1-methylcyclohexen-3-yl)-1,3-di(methoxymethoxy)olivetol (4)

In a round-bottom flask, a *cis–trans*-mixture of (4-acetyl-1-methylcyclohexen-3-yl)-1,3-di(methoxymethoxy)-olivetole (**3**) (100 mg; 0.45 mmol) was dissolved in toluene (10 mL). The solution was cooled to −10 °C before adding DIBAL-H (1.2 m in toluene; 0.31 mL). The solution was stirred at −10 °C for 2 h before quenching the reaction with a concentrated solution of potassium sodium tartrate (5 mL). The organic phase was separated, and the aqueous phase was extracted with toluene. All volatile compounds were removed under reduced pressure and the resident was purified by flash chromatography (eluent: hexane/ethyl acetate 8/1; r_f = 0.34).

Trans: **^{1}H-NMR** (400 MHz, CD_2Cl_2): δ = 6.60–6.67 (m, 2H, H-6, 4), 4.88–5.28 (m, 5H, H-2′, 1-OCH_2OCH$_3$, 3-OCH_2OCH$_3$), 3.53–4.33 (m, 2H, H-4′-C*H*CH$_3$OH, 3′), 3.38–3.49 (m, 6H, H-1-OCH$_2$OCH_3, 3-OCH$_2$OCH_3), 2.48–2.56 (m, 2H, H-1″), 1.72–2.36 (m, 5H, H-6′, 5′, 4′), 1.68 (s, 3H, H-1′-CH_3), 1.59 (s, 2H, H-2″), 1.30–1.36 (m, 4H, H-3″, 4″), 1.05 (d, J = 6.2 Hz, 3H, H-4′-CHCH_3OH), 0.88–0.92 (m, 3H, H-5″) ppm.

^{13}C-NMR (101 MHz, CD_2Cl_2): δ = 158.4 (C-3, 1), 144.0 (C-5), 133.3 (C-1′), 123.2 (C-2′), 118.2 (C-2), 109.0 (C-6, 4), 95.5 (C-1-O*C*H$_2$OCH$_3$, 3-O*C*H$_2$OCH$_3$), 70.4 (C-4′-*C*HCH$_3$OH), 56.7 C-1-OCH$_2$O*C*H$_3$, 3-OCH$_2$O*C*H$_3$), 47.8 (C-4′), 36.6 (C-1″), 33.3 (C-3′), 32.2 (C-3″), 31.6 (C-2″), 30.7 (C-6′), 24.0 (C-5′), 23.1 (C-1′-*C*H$_3$), 22.9 (C-4″), 21.1 (C-4′-CH*C*H$_3$OH), 14.4 (C-5″) ppm.

MS: m/z [M + Na]$^+$ = 429.28.

Retention time: 28.2 min.

Cis: **^{1}H-NMR** (400 MHz, CD_2Cl_2): δ = 6.57 (s, 2H, H-6, 4), 5.03–5.15 (m, 5H, H-2′, 1-OCH_2OCH$_3$, 3-OCH_2OCH$_3$), 3.73–3.81 (m, 1H, H-3′), 3.54–3.61 (m, 1H, H-4′-C*H*CH$_3$OH), 3.43 (s, 6H, H-1-OCH$_2$OCH_3, 3-OCH$_2$OCH_3), 2.48–2.54 (m, 2H, H-1″), 2.24–2.34 (m, 1H, H-4′), 2.08–2.20 (m, 1H, H-6′), 1.95–2.04 (m, 1H, H-6′), 1.85–1.92 (m, 1H, H-5′), 1.65 (s, 3H, H-1′-CH_3), 1.55–1.61 (m, 2H, H-2″), 1.44 (dd, J = 12.3 Hz, J = 5.1 Hz, 1H, H-5′), 1.28–1.37 (m, 4H, H-3″, 4″), 1.05 (d, J = 6.4 Hz, 3H, H-4′-CHCH_3OH), 0.86–0.93 (m, 3H, H-5″) ppm.

^{13}C-NMR (101 MHz, CD_2Cl_2): δ = 156.7 (C-1, 3), 143.3 (C-5), 132.5 (C-1′), 125.9 (C-2′), 120.7 (C-2), 109.1 (C-4, 6), 95.3 (C-1-O*C*H$_2$OCH$_3$, 3-O*C*H$_2$OCH$_3$), 70.6 (C-4′-*C*HCH$_3$OH), 56.5 (C-1-OCH$_2$O*C*H$_3$, 3-OCH$_2$O*C*H$_3$), 44.2 (C-4′), 36.7 (C-1″), 35.7 (C-3′), 32.2 (C-3″), 31.7 (C-2″), 30.8 (C-6′), 24.4 (C-5′), 23.7 (C-1′-*C*H$_3$), 23.1 (C-4″), 18.9 (C-4′-CH*C*H$_3$OH), 14.4 (C-5″) ppm.

MS: m/z [M + Na]$^+$ = 429.28.

Retention time: 28.1 min.

Flow synthesis of (4-acetyl-1-methylcyclohexen-3-yl)-1,3-di(methoxymethoxy)olivetol (3)

(*E*)-1,3-Bis(methoxymethoxy)-(3-methylbuta-1,3-dien-1-yl)-olivetole (**1**) (50.0 mg; 0.15 mmol) was dissolved in wet toluene (5 mL) and methyl vinyl ketone (**2**) (0.015 mL; 0.18 mmol) was added to the premixed solution before injecting 0.45 mL of the combined reagents into the loop (total volume = 0.45 mL). The desired temperature was set, and the reactor was heated up to the set temperature before injecting the reactant. Depending on the desired residence time, the flow rates were adjusted. The pressure has been set at 7 bar. For each condition, a sample was collected in an open flask and analyzed by gas chromatography.

Flow synthesis of (4-(1-hydroxyethyl)-1-methylcyclohexen-3-yl)-1,3-di(methoxymethoxy)olivetol (4)

(4-Acetyl-1-methylcyclohexen-3-yl)-1,3-di(methoxymethoxy)-olivetole (**3**) (20 mg; 0.05 mmol) was dissolved in toluene (2 mL) and injected through a 0.45 mL loop into the continuous flow of DIBAL-H (1 M in toluene, 1.5 eq.) after cooling the reactor to −10 °C. Depending on the desired residence time, die flow rates were adjusted, the flow rate of DIBAL-H was

adjusted to 1.5 equivalents. After the reactor, the reaction mixture was collected in a vessel filled with a concentrated solution of potassium sodium tartrate to quench the reaction. The organic phase was separated, and the aqueous phase was extracted with toluene. The combined organic phases were dried over sodium sulfate and concentrated under vacuum. Column chromatographic purification yielded the desired product.

Conclusions

We were able to design and manufacture several stainless-steel (316L) microflow reactors. All reactors could be printed using a standard desktop FDM printer. Depending on the size of the reactor, the total costs of one reactor, including the material and sintering process, are between 50 € and 100 €. This technique makes them easily accessible and customizable for any research facility. Due to the good thermal conductivity, the reactors can be easily heated or cooled to control the temperature of the reaction. For this purpose, we have developed a very compact and easy-to-use device. The controlling device could be built out of conventionally available and inexpensive electronic components and 3D-printed parts. We designed a central PCB, which could be purchased inexpensively and simplifies the soldering part. With the control unit, we could control a Peltier element or a PTC-heating thermistor. Both heating and cooling could be controlled simultaneously. With this setup, it was possible to reach reactor temperatures from −20 °C up to 200 °C. In addition to its excellent thermal conductivity, stainless steel is, due to its chemical stability to a wide range of compounds, particularly suitable as a material for flow reactors. To evaluate the functionality of the flow setup, we successfully carried out a Diels–Alder reaction between methyl vinyl ketone and a cannabinoid derivative at elevated temperatures, followed by a low-temperature reduction of the resulting carbonyl group using DIBAL-H in very good yields.

Conflicts of interest

There are no conflicts to declare.

Data availability

The data supporting this article have been included as part of the supplementary information (SI). Supplementary information: 3D printer setup, numbered part lists, detailed step-by-step assembly instructions, electronic setups of all components and NMR spectra of the synthesized compounds are described in the SI (PDF file). Gerber files, Arduino and Nextion program files and CAD files for 3D printing can be found in the SI (ZIP file). See DOI: https://doi.org/10.1039/d5re00326a.

Acknowledgements

We thank the Karl und Anna Buck Stiftung for funding this work. We acknowledge support by Open Access Publishing Fund of University of Tübingen.

Notes and references

1 M. B. Plutschack, B. Pieber, K. Gilmore and P. H. Seeberger, *Chem. Rev.*, 2017, **117**, 11796–11893.
2 K. B. Feng, Y. Y. Zhu, S. X. Gu, J. Long and H. F. Wang, *Asian J. Org. Chem.*, 2025, **14**, e202500132.
3 L. Capaldo, Z. Wen and T. Noël, *Chem. Sci.*, 2023, **14**, 4230–4247.
4 L. Y. Vázquez-Amaya, G. A. Coppola, E. V. Van der Eycken and U. K. Sharma, *J. Flow Chem.*, 2024, **14**, 257–279.
5 B. Gutmann and C. O. Kappe, *J. Flow Chem.*, 2017, **7**, 65–71.
6 J. Wegner, S. Ceylan and A. Kirschning, *Chem. Commun.*, 2011, **47**, 4583–4592.
7 A. S. Burange, S. M. Osman and R. Luque, *iScience*, 2022, **25**, 103892.
8 M. Movsisyan, E. I. P. Delbeke, J. K. E. T. Berton, C. Battilocchio, S. V. Ley and C. V. Stevens, *Chem. Soc. Rev.*, 2016, **45**, 4892–4928.
9 A. G. Niculescu, C. Chircov, A. C. Bîrcă and A. M. Grumezescu, *Int. J. Mol. Sci.*, 2021, **22**, 2011.
10 G. K. Monia Kabandana, T. Zhang and C. Chen, *Anal. Methods*, 2022, **14**, 2885–2906.
11 A. J. Capel, R. P. Rimington, M. P. Lewis and S. D. R. Christie, *Nat. Rev. Chem.*, 2018, **2**, 422–436.
12 A. J. N. Price, A. J. Capel, R. J. Lee, P. Pradel and S. D. R. Christie, *J. Flow Chem.*, 2021, **11**, 37–51.
13 O. A. Alimi and R. Meijboom, *J. Mater. Sci.*, 2021, **56**, 16824–16850.
14 F. Menzel, T. Klein, T. Ziegler and J. M. Neumaier, *React. Chem. Eng.*, 2020, **5**, 1300–1310.
15 J. Zheng, Y. Niu, Z. Song, N. Li and S. Ju, *JOM*, 2025, **77**, 415–430.
16 M. A. Ali, C. Hu, E. A. Yttri and R. Panat, *Adv. Funct. Mater.*, 2022, **32**, 2107671.
17 M. S. Hassan, S. Zaman, J. Z. R. Dantzler, D. H. Leyva, M. S. Mahmud, J. M. Ramirez, S. G. Gomez and Y. Lin, *Nanomaterials*, 2023, **13**, 3148.
18 S. Waheed, J. M. Cabot, N. P. Macdonald, T. Lewis, R. M. Guijt, B. Paull and M. C. Breadmore, *Lab Chip*, 2016, **16**, 1993–2013.
19 J. M. Neumaier, A. Madani, T. Klein and T. Ziegler, *Beilstein J. Org. Chem.*, 2019, **15**, 558–566.
20 P. J. Kitson, S. Glatzel, W. Chen, C.-G. Lin, Y.-F. Song and L. Cronin, *Nat. Protoc.*, 2016, **11**, 920–936.
21 A. Enders, I. G. Siller, K. Urmann, M. R. Hoffmann and J. Bahnemann, *Small*, 2019, **15**, 1804326.
22 C. Y. Yap, C. K. Chua, Z. L. Dong, Z. H. Liu, D. Q. Zhang, L. E. Loh and S. L. Sing, *Appl. Phys. Rev.*, 2015, **2**, 041101.
23 U. Aziz, M. McAfee, I. Manolakis, N. Timmons and D. Tormey, *Materials*, 2025, **18**, 2870.

24 S. Roos and L.-E. Rännar, *Metals*, 2021, **11**, 137.
25 S. Mirzababaei and S. Pasebani, *J. Manuf. Mater. Process.*, 2019, **3**, 82.
26 J. Kráľ, T. Dzuro and H. Debski, *Materials*, 2024, **17**, 4400.
27 F. Grinschek, S. Dübal, C. Klahn and R. Dittmeyer, *Chem. Ing. Tech.*, 2022, **94**, 958–966.
28 M. Lämmermann, G. Horak, W. Schwieger and H. Freund, *Chem. Eng. Process.*, 2018, **126**, 178–189.
29 A. Avril, C. H. Hornung, A. Urban, D. Fraser, M. Horne, J. P. Veder, J. Tsanaktsidis, T. Rodopoulos, C. Henry and D. R. Gunasegaram, *React. Chem. Eng.*, 2017, **2**, 180–188.
30 T. Wolf, Z. Fu and C. Körner, *Mater. Lett.*, 2019, **238**, 241–244.
31 M. C. Maier, R. Lebl, P. Sulzer, J. Lechner, T. Mayr, M. Zadravec, E. Slama, S. Pfanner, C. Schmölzer, P. Pöchlauer, C. O. Kappe and H. Gruber-Woelfler, *React. Chem. Eng.*, 2019, **4**, 393–401.
32 G. Scotti, S. M. E. Nilsson, V.-P. Matilainen, M. Haapala, G. Boije af Gennäs, J. Yli-Kauhaluoma, A. Salminen and T. Kotiaho, *Heliyon*, 2019, **5**, e02002.
33 B. Gutmann, M. Köckinger, G. Glotz, T. Ciaglia, E. Slama, M. Zadravec, S. Pfanner, M. C. Maier, H. Gruber-Wölfler and C. Oliver Kappe, *React. Chem. Eng.*, 2017, **2**, 919–927.
34 H.-J. Kim, K. Mori, T. Nakano and H. Yamashita, *Catal. Sci. Technol.*, 2025, **15**, 669–672.
35 N. Mohammad, R. Y. Abrokwah, R. G. Stevens-Boyd, S. Aravamudhan and D. Kuila, *Catal. Today*, 2020, **358**, 303–315.
36 H. Gong, C. Crater, A. Ordonez, C. Ward, M. Waller and C. Ginn, *MATEC Web Conf.*, 2018, **249**, 01001.
37 M. Á. Caminero, A. Romero, J. M. Chacón, P. J. Núñez, E. García-Plaza and G. P. Rodríguez, *Rapid Prototyp. J.*, 2021, **27**, 583–591.
38 A. A. Dos-Reis-Delgado, A. Carmona-Dominguez, G. Sosa-Avalos, I. H. Jimenez-Saaib, K. E. Villegas-Cantu, R. C. Gallo-Villanueva and V. H. Perez-Gonzalez, *Electrophoresis*, 2023, **44**, 268–297.
39 Y. H. Ting, *IEEE Trans. Ind. Appl.*, 1972, **IA-8**, 338–344.
40 T. Pardy and T. Rang, *WIT Trans. Eng. Sci.*, 2015, **90**, 263–271.
41 P. M. Peltier, *Ann. Chim. Phys.*, 1834, **56**, 371–386.
42 M.-K. Shilpa, M.-A. Raheman, A. Aabid, M. Baig, R.-K. Veeresha and N. Kudva, *Fluid Dyn. & Mater. Process.*, 2023, **19**, 187–206.
43 C. Wang, W. Mai, Q. Shi, Z. Liu, Q. Pan and J. Peng, *J. Mater. Eng. Perform.*, 2023, **33**, 11781–11793.
44 M. Sarzynski, P. Platek, P. Cedro, U. Gunputh, P. Wood and A. Rusinek, *Materials*, 2024, 17.
45 F. Menzel, J. Cotton, T. Klein, A. Maurer, T. Ziegler and J. M. Neumaier, *J. Flow Chem.*, 2023, **13**, 247–256.
46 F. Korte, E. Dlugosch and U. Claussen, *Justus Liebigs Ann. Chem.*, 1966, **693**, 165–170.